





## COMPARATIVE ANALYSIS OF NESTED DOMAIN SENSITIVITY ON THUNDERSTORM SIMULATION USING WRF-ARW MODEL: A CASE STUDY OVER BANGLADESH

 **Md. Mijanur Rahman**<sup>1\*</sup>

 **Muhammad Abul Kalam Mallik**<sup>2</sup>

 **Md. Abdus Samad**<sup>3</sup>

<sup>1</sup>Lecturer, Department of Applied Mathematics, University of Dhaka, Dhaka, Bangladesh.

Email: [mmr.apmath@du.ac.bd](mailto:mmr.apmath@du.ac.bd) Tel: +8801515632293

<sup>2</sup>Meteorologist, Storm Warning Centre, Bangladesh Meteorological Department, Dhaka, Bangladesh.

Email: [mallikak76@yahoo.com](mailto:mallikak76@yahoo.com) Tel: +8801711048157

<sup>3</sup>Professor, Department of Applied Mathematics, University of Dhaka, Dhaka, Bangladesh.

Email: [samad@du.ac.bd](mailto:samad@du.ac.bd) Tel: +8801552433642



(+ Corresponding author)

### ABSTRACT

#### Article History

Received: 28 January 2021

Revised: 22 February 2021

Accepted: 16 March 2021

Published: 7 April 2021

#### Keywords

Thunderstorm  
Bangladesh  
WRF-ARW model  
Nested domain  
Thunderstorm indicators  
Numerical weather prediction.

Several thunderstorm indicators (TI) and thermodynamic features were evaluated and compared by simulating a thunderstorm (TS) event over Sylhet (24.89° N, 91.86° E), Bangladesh that occurred from 1429 UTC to 1441 UTC on 29 March 2018 using the Advanced Research dynamics solver of Weather Research and Forecasting model (WRF-ARW). The model was run to conduct a simulation for 36 hours utilizing six-hourly Global Final Analysis (FNL) datasets from 0600 UTC of 29 March 2018 to 1200 UTC of 30 March 2018 as initial and lateral boundary conditions. The domain was nested in two different ways: (a) two domains of 15 and 3 km horizontal resolution, and (b) three domains of 12, 6 and 3 km horizontal resolution. These domains were nested with varying outer-domain horizontal grid spacing but a constant 3km inner-domain resolution in order to reasonably verify the effect of nesting on the approximation of the thermodynamic indicators by WRF-ARW. The model outputs were generated with a 10-minute interval for the innermost domain. These outputs were analyzed numerically and graphically using Grid Analysis and Display System (GrADS). Model evaluations of mean sea level pressure (MSLP), maximum and minimum temperature, relative humidity (RH) and 24-hour rainfall were compared with available observational data obtained from Bangladesh Meteorological Department (BMD) to validate the model performance in each case. Based on the analyses and comparisons, it is found that the estimated values in the case of three-way nesting were better indicators of the likelihood of a TS event over that area.

**Contribution/Originality:** This study is one of the very few studies that estimate several important thunderstorm indicators of a thunderstorm event over Bangladesh using the WRF-ARW model. This paper's major contribution is the comparative analysis of those indicators based on different nested domain configurations.

### 1. INTRODUCTION

How the Earth's atmosphere works and changes have eluded humans for a long time – not only for curiosity but also because many aspects of human life are directly related to weather. That's why scientists did – and are still doing – a tremendous amount of research to understand and predict its complex behavior. Thunderstorm (TS) is one of the most complicated and devastating phenomena in it. TS is caused by vigorous convective dynamics and characterized by lightning and thunder associated with stormy winds, heavy rainfall, hail and tornadoes. It is very

common over Bangladesh ( $20^{\circ}34' \text{ N}$  to  $26^{\circ}38' \text{ N}$  and  $88^{\circ}01' \text{ E}$  to  $92^{\circ}41' \text{ E}$ ) during the pre-monsoon season. TS is locally known as 'Kal-baishakhi' in Bengali: 'Kal' means something dangerous and evil signifying the heavy damage to life and property due to TS and 'baishakhi' indicates the month of 'Baishakh' – the first month of the Bengali calendar (from mid-April to mid-May) during which TS occurs most frequently. Bangladesh has an estimate of 60 to 100 TS days per year [1] and it is the 3<sup>rd</sup> most violent hazard affecting lives and properties in Bangladesh [2].

Due to the smaller spatial and temporal continuance of TS than other large scale weather phenomena like tropical cyclone or monsoon together with the inherent non-linear nature of the dynamics of TS, forecasting it – even over a particular region – has always been one of the most daunting challenges for meteorologists. Recently, the introduction of Numerical Weather Prediction (NWP) systems to aid conventional techniques has improved TS forecasting to a great extent. The physics and dynamics of a TS can be understood by simulating various associated thermodynamic features with the help of NWP systems such as the Global Forecast System (GFS) and WRF model. Such attempts with high-resolution mesoscale models over the Indo-Bangla region has been made mainly in the past fifteen years. Vaidya [3] studied the simulation of a pre-monsoon thunderstorm over the east coast of India using mesoscale models. Chatterjee, et al. [4] used mesoscale model MM5 to simulate two hailstorm events over the Gangetic Plain of West Bengal. The authors found that the model MM5 with suitable modification to the cloud microphysics scheme of Schultz has the ability to simulate hailstorms considerably. The Nonhydrostatic Mesoscale Model (NMM) core of the WRF was used to perform a simulation of a severe thunderstorm event by Litta and Mohanty [5]. Basnayake [6] studied the observations and WRF simulations of pre-monsoon nor'westers in 2009 over Bangladesh and adjoining regions in the neighborhood. Rajeevan, et al. [7] investigated the sensitivity of four different microphysics (MP) schemes in WRF simulation of a severe thunderstorm event over Gadanki (southeast India). This study showed large sensitivity of the microphysics schemes in the simulations of thunderstorms by the WRF model. Das [8] analyzed the effect of observational data assimilation in the WRF model on the simulation of thunderstorms in his SMRC [9] also studied the sensitivity of physical parameterization schemes in the simulation of mesoscale convective systems associated with squall events using the WRF-ARW model. Simulations of TS events over the East Indian region using WRF-NMM and WRF-ARW cores were compared by Litta, et al. [10]. Ahasan, et al. [11] performed a simulation of a TS event that occurred over Srimangal, Bangladesh at 1200 UTC on 21 May 2011 using WRF-ARW model. Their simulation overestimated the 24-hour rainfall by 46.72% compared to the observation recorded by Bangladesh Meteorological Department (BMD). Bandyopadhyay, et al. [12] discussed the dynamics of severe weather events over the SAARC region. Ahasan and Debsarma [13] studied the impact of data assimilation in simulation of a squall line that occurred on 11 May 2011 over Bangladesh using WRF model. However, the effect of nesting on the simulation of TS over Bangladesh has not yet been done.

In this paper, six TS indicators, as well as several thermodynamic features, are evaluated by simulating the TS event that occurred over Sylhet ( $24.89^{\circ} \text{ N}$ ,  $91.86^{\circ} \text{ E}$ ) from 1429 UTC to 1441 UTC on 29 March 2018 using the WRF-ARW model. Two different ways of nesting for the study region were used: one consisting of two domains of 15 km (outer) and 5 km (inner), and another consisting of three domains of 12 km (outer), 9 km (middle) and 3 km (inner). Over each innermost domain, six thunderstorm indicators namely, Convective Available Potential Energy (CAPE), Storm Relative Helicity (Hs-r), K Index (KI), Total Totals Index (TT), reflectivity, and 500 hPa wind were evaluated and compared numerically. Graphical analyses were done using GrADS. Along with these six indicators, mean sea level pressure (MSLP), relative humidity (RH), temperature and rainfall were simulated, analyzed and compared graphically with observational data obtained from Bangladesh Meteorological Department (BMD).

## 2. METHODOLOGY

### 2.1. Data

Six-hourly Global Final Analysis (FNL) datasets, formatted as the second version of General Regularly-distributed Information in Binary form (GRIB2), from 0600UTC of 29 March 2018 to 1200UTC of 30 March 2018

were used during the simulation as the initial and lateral boundary conditions. These data are prepared by National Center for Environmental Prediction (NCEP) on  $1^\circ$  by  $1^\circ$  grid operationally every six hours from the Global Data Assimilation System (GDAS). GDAS continuously collects observational data from the Global Telecommunications System (GTS), and other sources, for many analyses. These analyses are available on the surface, at 26 mandatory pressure levels from 1000 hPa to 10 hPa, in the surface boundary layer and at some sigma layers, the tropopause and a few others. On the other hand, available observations of MSLP, maximum and minimum temperature, RH and rainfall amount of the event day were collected from the archive of BMD to validate the model derived simulation.

## 2.2. WRF Model Configuration

The WRF model is a non-hydrostatic mesoscale model developed for simulation and prediction of atmospheric phenomena of different scales, emphasizing horizontal grid lengths of a few kilometers or less [14]. It has two dynamics solvers: Advanced Research WRF (ARW) and Nonhydrostatic Mesoscale Model (NMM). ARW (version 4.1) developed by the National Center for Atmospheric Research (NCAR) [15] is implemented during this study. The two different types of nesting used in this study are shown in Figure 1(a-b).

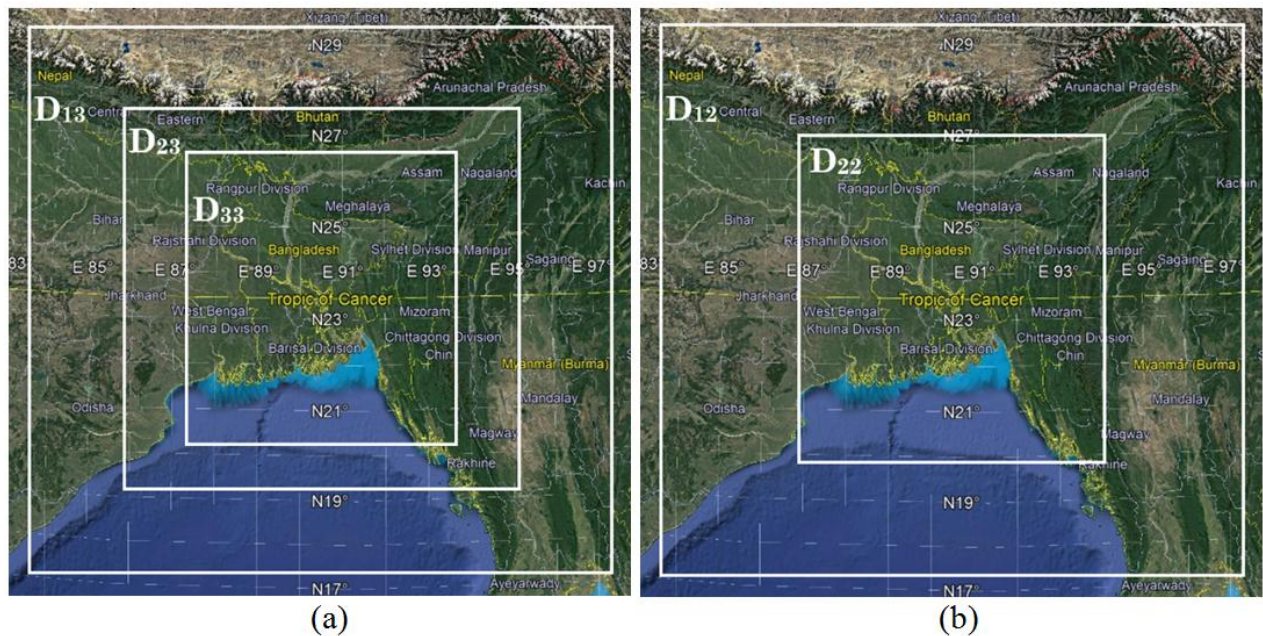


Figure-1(a). Two nested domains, (b) Three nested domains.

The center of each domain was taken to be  $23.5^\circ$  N &  $90.5^\circ$  E. For convenience, we label the domains as  $D_{ij}$  which denotes the  $i^{th}$  domain of  $j$  nested domains. Thus the outer domain of Figure 1(a) is labelled  $D_{12}$  since it is the first domain of 2 nested domains. Similarly, the outer domain of Figure 1(b) is labelled as  $D_{13}$  and so on. Details of the domain configuration used in this study are given in Table 1. The WRF model is equipped with numerous schemes for the physical investigation of different dynamics such as microphysics, radiation physics, planetary boundary layer (PBL) physics and cloud physics (cumulus parametrization). The detailed configuration of the model used for the simulations in this study is given in Table 2.

**Table-1.** Details of the domain configuration used in this study.

Type	(a)		(b)	
	Nested		Nested	
Number of domains	Two		Three	
Central coordinate	23.5° N, 90.5° E		23.5° N, 90.5° E	
Total covered area	D <sub>12</sub> :	17.30°N – 29.42°N, 83.58°E – 97.42°E	D <sub>13</sub> :	17.38°N – 29.35°N, 83.55°E – 97.45°E
	D <sub>22</sub> :	19.90°N – 27.00°N, 86.92°E – 94.08°E	D <sub>23</sub> :	19.25°N – 27.61°N, 85.88°E – 95.11°E
Horizontal resolution	D <sub>12</sub> : 15km × 15km D <sub>22</sub> : 3km × 3km		D <sub>13</sub> :	12km × 12km
			D <sub>23</sub> :	6km × 6km
Grid size	D <sub>12</sub> : 95 × 91 × 40 D <sub>22</sub> : 245 × 265 × 40		D <sub>33</sub> :	3km × 3km
			D <sub>13</sub> :	119 × 112 × 40
Integration time step	D <sub>12</sub> : 75 seconds D <sub>22</sub> : 15 seconds		D <sub>23</sub> :	158 × 156 × 40
			D <sub>33</sub> :	220 × 240 × 40
Output data interval	D <sub>12</sub> : 50 min D <sub>22</sub> : 10 min		D <sub>13</sub> :	60 seconds
			D <sub>23</sub> :	30 seconds
			D <sub>33</sub> :	15 seconds
			D <sub>13</sub> :	80 min
			D <sub>23</sub> :	40 min
			D <sub>33</sub> :	10 min

**Table-2.** Details of the WRF Model configuration used in this study.

Dynamics	
WRF core	ARW
Input data type	NCEP–FNL
Input data interval	6 hours
Map projection	Mercator
Vertical coordinates	Pressure coordinate
No. of vertical levels	40
Time integration scheme	Runge-Kutta 3 <sup>rd</sup> order method (RK-3)
Spatial differencing scheme	Centered difference 6 <sup>th</sup> order formula
Physics	
Microphysics	Kessler scheme
PBL parameterization	Yonsei University (YSU) scheme
Surface layer physics	Revised MM5 scheme
Land-surface model	Unified Noah LSM
Short-wave radiation	Dudhia scheme
Long-wave radiation	RRTM scheme
Cumulus parameterization	Kain–Fritsch (new Eta) scheme

### 3. GOVERNING EQUATIONS

The basic form of the atmospheric governing equations are as follows:

$$\frac{du}{dt} - \frac{uv \tan \phi}{a} + \frac{uw}{a} = -\frac{1}{\rho} \frac{\partial p}{\partial x} + 2\Omega v \sin \phi - 2\Omega w \cos \phi + F_x \quad (1a)$$

$$\frac{dv}{dt} + \frac{u^2 \tan \phi}{a} + \frac{vw}{a} = -\frac{1}{\rho} \frac{\partial p}{\partial y} - 2\Omega u \sin \phi + F_y \quad (1b)$$

$$\frac{dw}{dt} - \frac{u^2 + v^2}{a} = -\frac{1}{\rho} \frac{\partial p}{\partial z} - g + 2\Omega u \cos \phi + F_z \quad (1c)$$

$$\frac{\partial \rho}{\partial t} = -\nabla \cdot (\rho \mathbf{U}) \quad (2)$$

$$p = \rho RT \quad (3)$$

$$c_p \frac{d \ln T}{dt} - R \frac{d \ln p}{dt} = \frac{J}{T} = \frac{ds}{dt} \quad (4)$$

$$\frac{dq}{dt} = E - C \quad (5)$$

The first three equations can be written compactly in vector form as follows:

$$\frac{d\mathbf{U}}{dt} = -\frac{1}{\rho} \nabla p + \mathbf{g} + \mathbf{F} - 2\boldsymbol{\Omega} \times \mathbf{U} \quad (6)$$

This is another form of momentum equation that states Newton's second law for a motion relative to a rotating coordinate frame. Here,  $\mathbf{U} = (u, v, w)$  is the velocity vector relative to the rotating frame,  $\rho$  is the density,  $p$  denotes pressure,  $\mathbf{g}$  is the acceleration due to gravity,  $\mathbf{F}$  represents the frictional force and centrifugal force combinedly and  $\boldsymbol{\Omega}$  is the angular velocity of the rotating frame. This equation states that the acceleration following the relative motion in the rotating frame equals the sum of the Coriolis force, the pressure gradient force, gravity, frictional and centrifugal force. The first three equations are applicable for a spherical coordinate system in which  $a$  is the mean radius of Earth while  $\phi$  denotes the latitude. Equations (1a), (1b) and (1c) are respectively the eastward, northward and vertical component of the momentum Equation (6). Equation (2) is the continuity equation that ensures the conservation of mass. It states that the local rate of change of density is equal to the convergence of mass. Equation (3) is called the equation of state (or ideal gas law) for dry air. In this equation,  $T$  denotes the temperature while  $R$  is the gas constant whose value for dry air is  $287 \text{ J kg}^{-1} \text{ K}^{-1}$ . In Equation (4),  $c_p$  is the specific heat at constant pressure,  $s$  designates entropy and  $J$  is the rate of heating per unit mass due to radiation, conduction and latent heat release. It indicates that vertical motion in the atmosphere changes the thermodynamic state in a reversible way. A parcel moving vertically will change temperature due to compression or expansion with pressure change, but when returned to its original level, it will have done no work on its environment. If  $J = 0$ , then its temperature will return to the original temperature. Equation (5) is the simplified form of the conservation of moisture which states that the rate of change of moisture following the motion of an air parcel  $\left(\frac{dq}{dt}\right)$  is equal to the difference between evaporation–sublimation ( $E$ ) and condensation ( $C$ ). The ARW



dynamics solver of the WRF model integrates the compressible, non-hydrostatic Euler equations. The equations are cast into flux form using transformation of variables that conserves all the properties following [16] and then reformulated using a terrain-following mass vertical coordinate [17]. After the inclusion of moisture effect, curvature terms and Coriolis effects, they are further augmented to include the projections to the sphere. Finally, the governing equations are recast into a perturbed form using perturbation variables to reduce truncation and rounding-off errors in calculations before constructing the discrete solver.

#### 4. SYNOPTIC CONDITION OF THE CASE STUDY

According to the records of BMD, a squall took place over Sylhet from 1429 UTC to 1320 UTC on 29 March 2018. A trough of westerly low was observed over Sylhet and the neighborhood on the event day. Mean Sea Level Pressure (MSLP) at 1200 UTC was observed to be 1004.6 hPa at Sylhet station. Powerful stormy wind was observed to be blowing from the west to the east with a maximum speed of  $92 \text{ km h}^{-1}$  (50 knots). An amount of 21 millimeters of rainfall was recorded at that station over the 24 hours of that day.

#### 5. SIMULATION

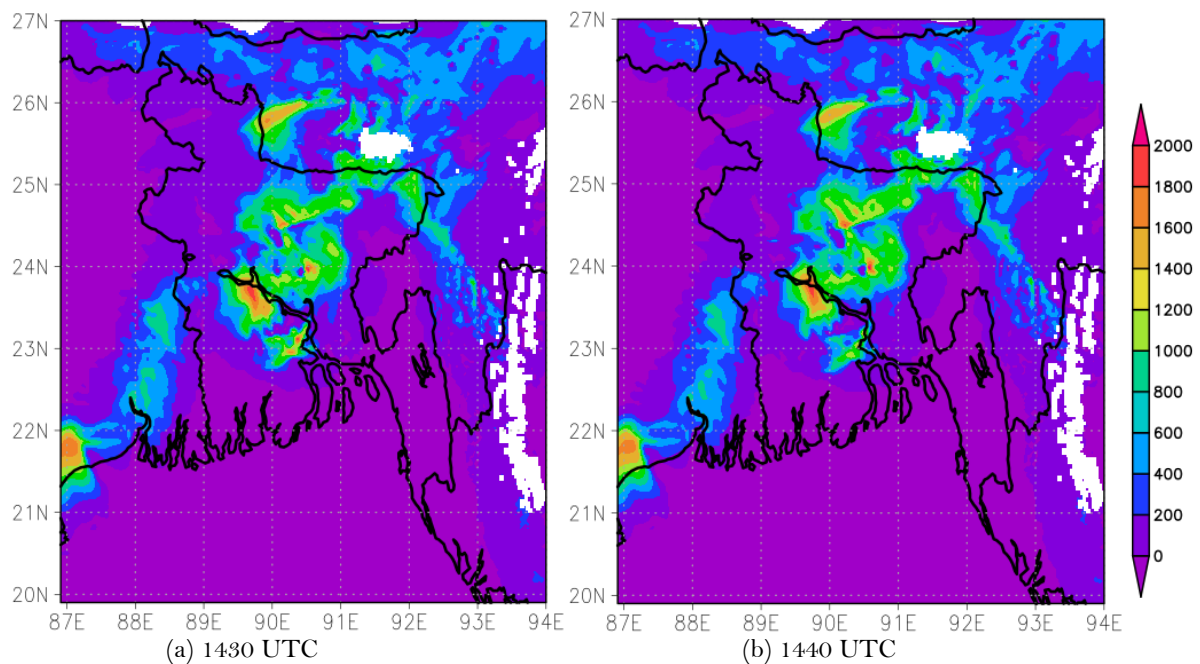
##### 5.1. CAPE

CAPE is the short form of ‘Convective Available Potential Energy’. It is a measure of the amount of energy available for convection. Mathematically, CAPE is calculated by integrating vertically the local buoyancy of a parcel from the level of free convection (LFC) to the equilibrium level (EL) according to the American Meteorological

Society [18] as follows:  $CAPE = \int_{p_f}^{p_n} R_d (T_{vp} - T_{ve}) d \ln p$ , where  $T_{vp}$  is the virtual temperature of a lifted

parcel moving upward moist adiabatically from LFC to EL,  $T_{ve}$  is the virtual temperature of the environment,  $R_d$

is the specific gas constant for dry air,  $p_f$  is the pressure at LFC, and  $p_n$  is the pressure at EL.



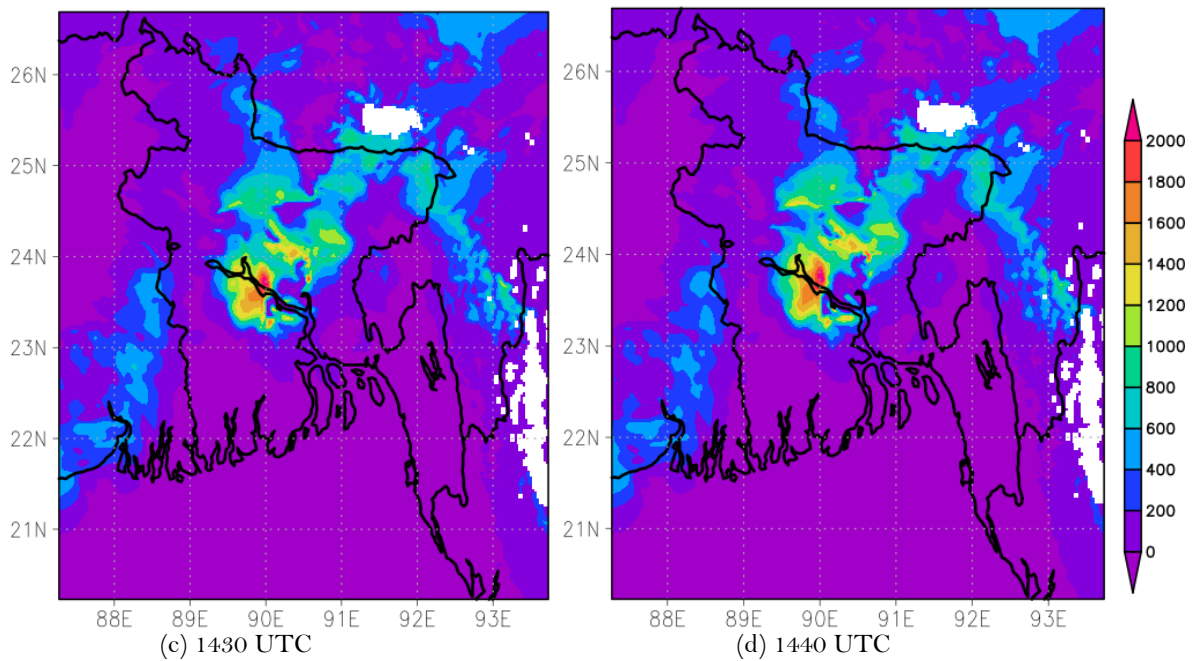


Figure-2. Simulated CAPE at 850 hPa level for domain  $D_{22}$  (a, b) and domain  $D_{33}$  (c, d).

Model-simulated CAPE at 850 hPa level based on the initial conditions of 0600 UTC of 29 March 2018 are shown in Figure 2(a, b) and Figure 2(c, d) for the domains  $D_{22}$  and  $D_{33}$  respectively. In the case of  $D_{22}$ , 800-1000  $J kg^{-1}$  CAPE is simulated over Sylhet at 1430 UTC which remains almost the same for the next 10 minutes. Similar values are simulated in the case of  $D_{33}$  also.

However, in  $D_{22}$ , strong CAPE values ( $>2000 J kg^{-1}$ ) is modeled in the north-western and south-western region of Sylhet, unlike  $D_{33}$  which shows higher values only in the south-western side. In both domains, CAPE is simulated to be increasing with time over these regions which is a strong indication of unstable weather and possible TS formation. Overall,  $D_{22}$  shows higher values of CAPE than  $D_{33}$ .

### 5.2. Storm Relative Helicity (Hs-r)

Storm relative helicity, abbreviated Hs-r, is an important TS index that estimates the potential of a thunderstorm to achieve a rotating updraft when there exists an environmental vertical wind shear profile.

It accumulates the effects of storm-relative winds and the horizontal vorticity that is generated by the vertical shear of the horizontal wind within the inflow layer of a storm. We simulated Hs-r at 1km and 3km levels in  $D_{22}$  and  $D_{33}$  which are shown in figure 3 and 4 respectively.

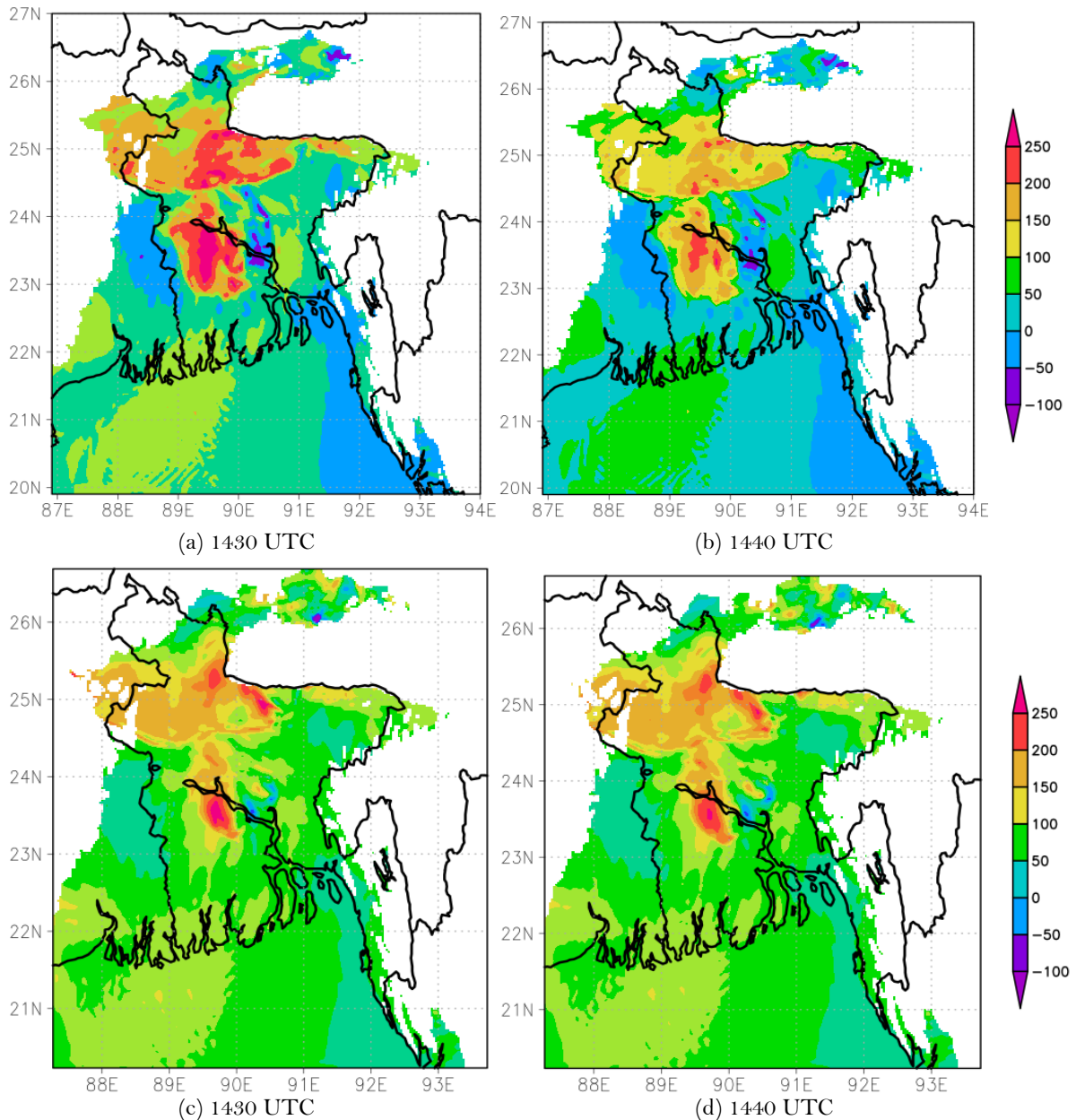


Figure-3. Simulated Hs-r at 1 km for domain  $D_{22}$  (a, b) and domain  $D_{33}$  (c, d).

Figure 3 (a, b) shows that in  $D_{22}$ , 1km Hs-r index is found to be between 0-50  $m^2 s^{-2}$  over Sylhet and above 150  $m^2 s^{-2}$  in the western and northern neighborhood. In the case of  $D_{33}$  (Figure 3(c, d)), higher values of Hs-r (50-100  $m^2 s^{-2}$ ) are seen over Sylhet but the neighboring regions have less Hs-r on average than that of  $D_{22}$  at 1430 UTC. But at 1440 UTC, the scenario is almost similar. Figure 4 (a, b) reflects negative Hs-r values at 3 km over Sylhet which is significantly lower than that of  $D_{33}$  (0-100  $m^2 s^{-2}$ ) as shown in Figure 4 (c, d). Also, the surrounding regions have more Hs-r index value for  $D_{33}$  than  $D_{22}$ . A higher Hs-r index suggests that there is a high chance of stronger storms. Thus,  $D_{33}$  captured this aspect better than  $D_{22}$  overall.



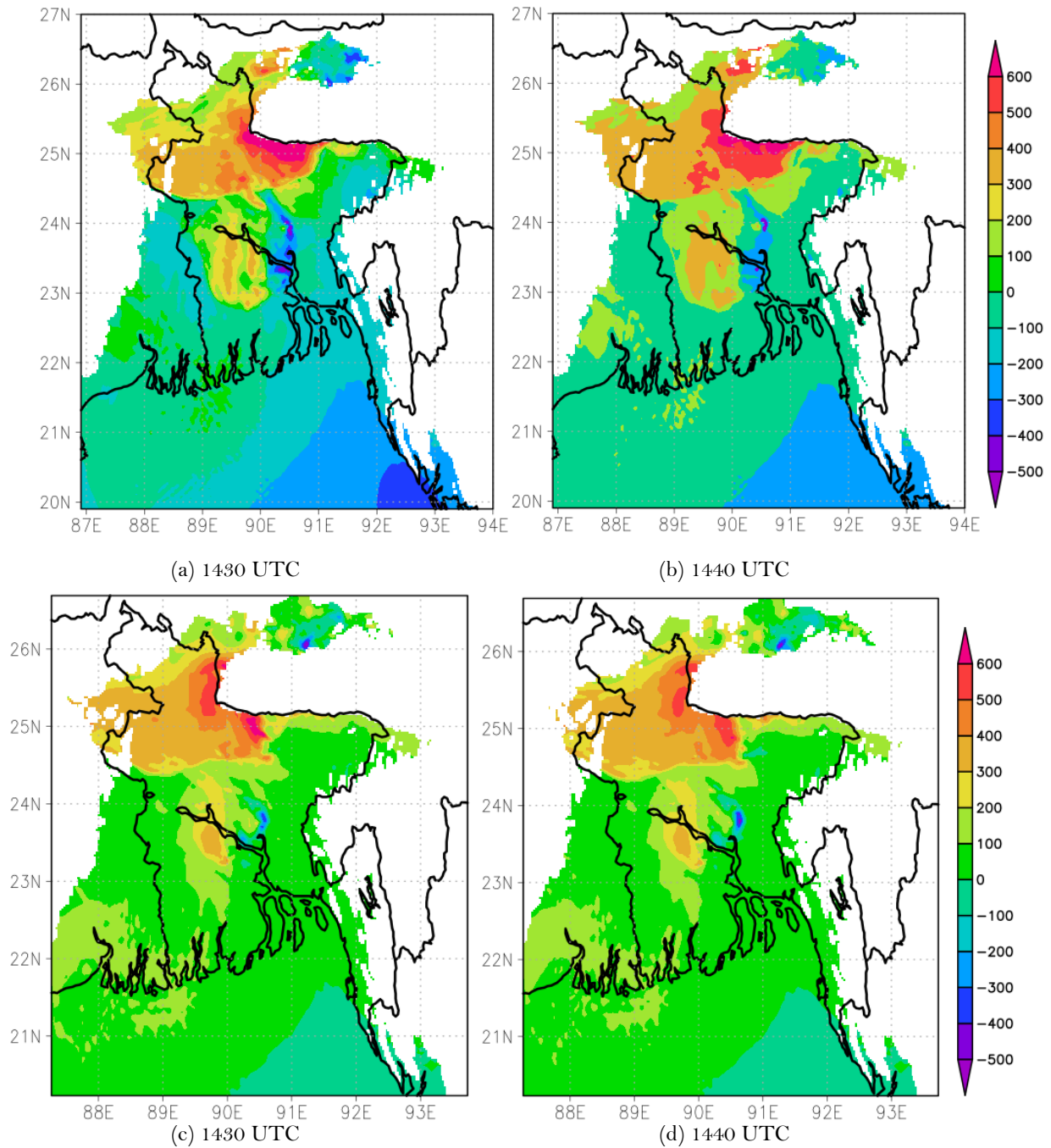


Figure-4. Simulated Hs-r at 3 km for domain  $D_{22}$  (a, b) and domain  $D_{33}$  (c, d).

### 5.3. K Index

The K index (KI) is a measure that expresses the potential of thunderstorms based on the lapse rate of temperature with respect to height, and the amount of low-level moisture in the atmosphere. K over  $30^{\circ}\text{C}$  indicates better potential for thunderstorms with heavy rain. WRF simulated K values are shown in Figure 5 (a, b) for  $D_{22}$  and in Figure 5 (c, d) for  $D_{33}$ .

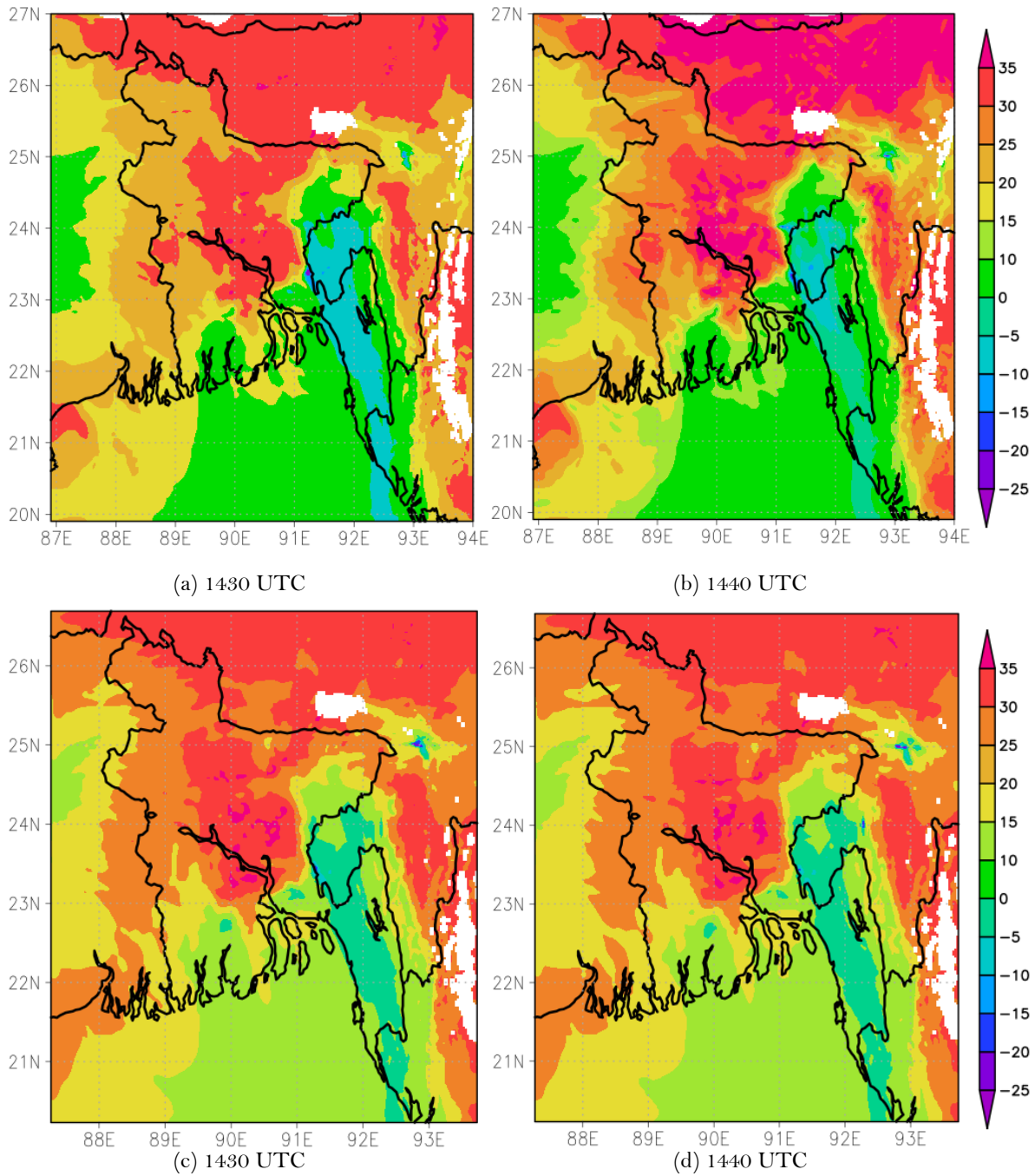


Figure-5. Simulated K index for domain  $D_{22}$  (a, b) and domain  $D_{33}$  (c, d).

It is found that, in  $D_{22}$ , K index is mostly 0-10°C over Sylhet and 10-20 in the surrounding areas as shown in Figure 5 (a, b). On the other, Figure 5 (c, d) for  $D_{33}$  shows a K index of 15-20°C over Sylhet and 25-35°C in the close neighborhood. That is, KI values for  $D_{33}$  is more indicative of potential TS than that of  $D_{22}$ .

#### 5.4. Total Totals Index

The Total Totals Index, abbreviated as TT, consists of two components: Vertical Totals (VT) and Cross Totals (CT). The VT represents the lapse rate between 850 and 500 hPa level and the CT is the difference between normal

and dewpoint temperature at 850 hPa level. Thus, TT accounts for static stability as well as 850 hPa moisture. TT values above 45°C indicate possible TS and more than 55°C TT suggests severe TS most likely.

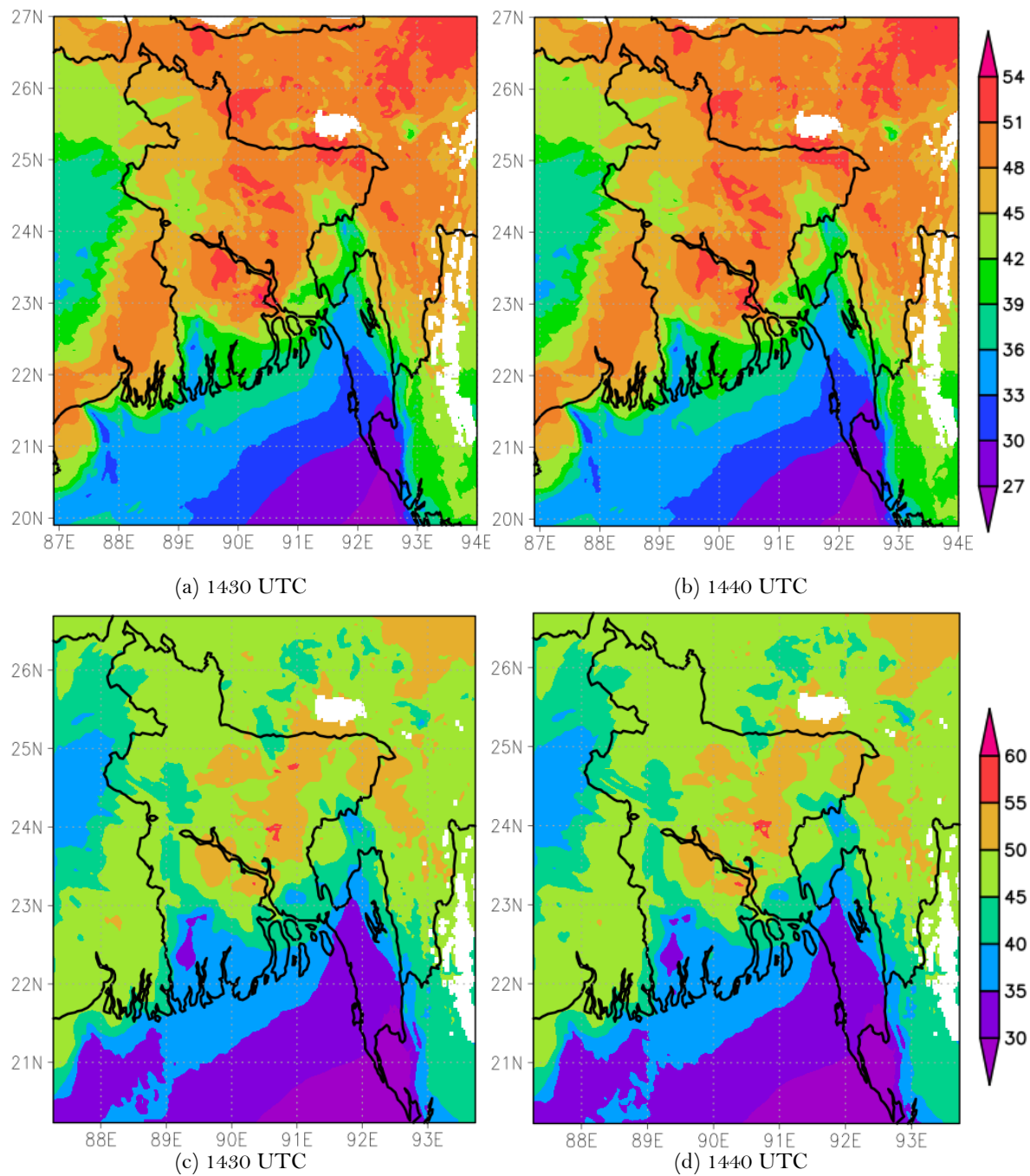


Figure-6. Simulated TT index for domain  $D_{22}$  (a, b) and domain  $D_{33}$  (c, d).

TT values simulated by the WRF model are shown in figure 6. In the case of  $D_{22}$ , as shown in Figure 6 (a, b), 48–54°C TT is simulated over Sylhet and its adjoining northern areas while in the case of  $D_{33}$  it is in the range 45–50°C. Therefore, the  $D_{22}$  estimate of this index is a better indicator of TS event over this area than that of  $D_{33}$ .

### 5.5. Reflectivity

Simulated Composite RADAR Reflectivity, simply called Reflectivity, forecasts what a weather radar may be showing considering the amount of water forecast to be in the atmosphere. It has a unit of dBZ which stands for decibel relative to Z. It's a dimensionless unit in the logarithmic scale used in weather radar to compare the equivalent reflectivity factor ( $Z$ ) of a remote object to the return of a droplet of rain [19].

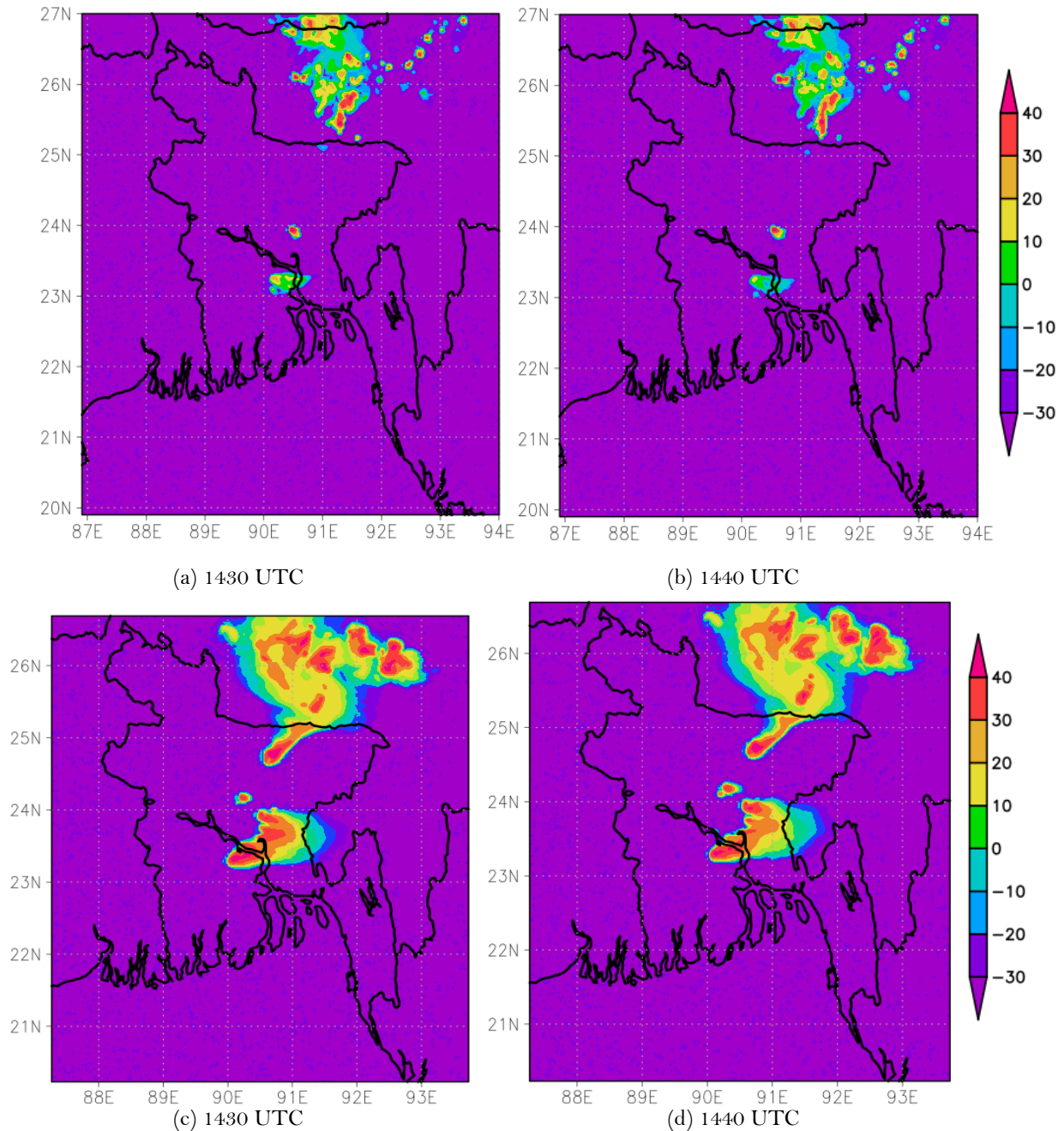


Figure-7. Simulated dBZ at 500 hPa level for domain  $D_{22}$  (a, b) and domain  $D_{33}$  (c, d).

It is a fairly good indicator of convection and the subsequent development of thunderstorms. Values above 40 dBZ indicate the likelihood of storms with hail and thunder. WRF simulated dBZ values at 500 hPa level are shown in Figure 7. We have also simulated vertical cross-sections of dBZ values along  $24.89^\circ\text{N}$  which are shown in Figure 8.



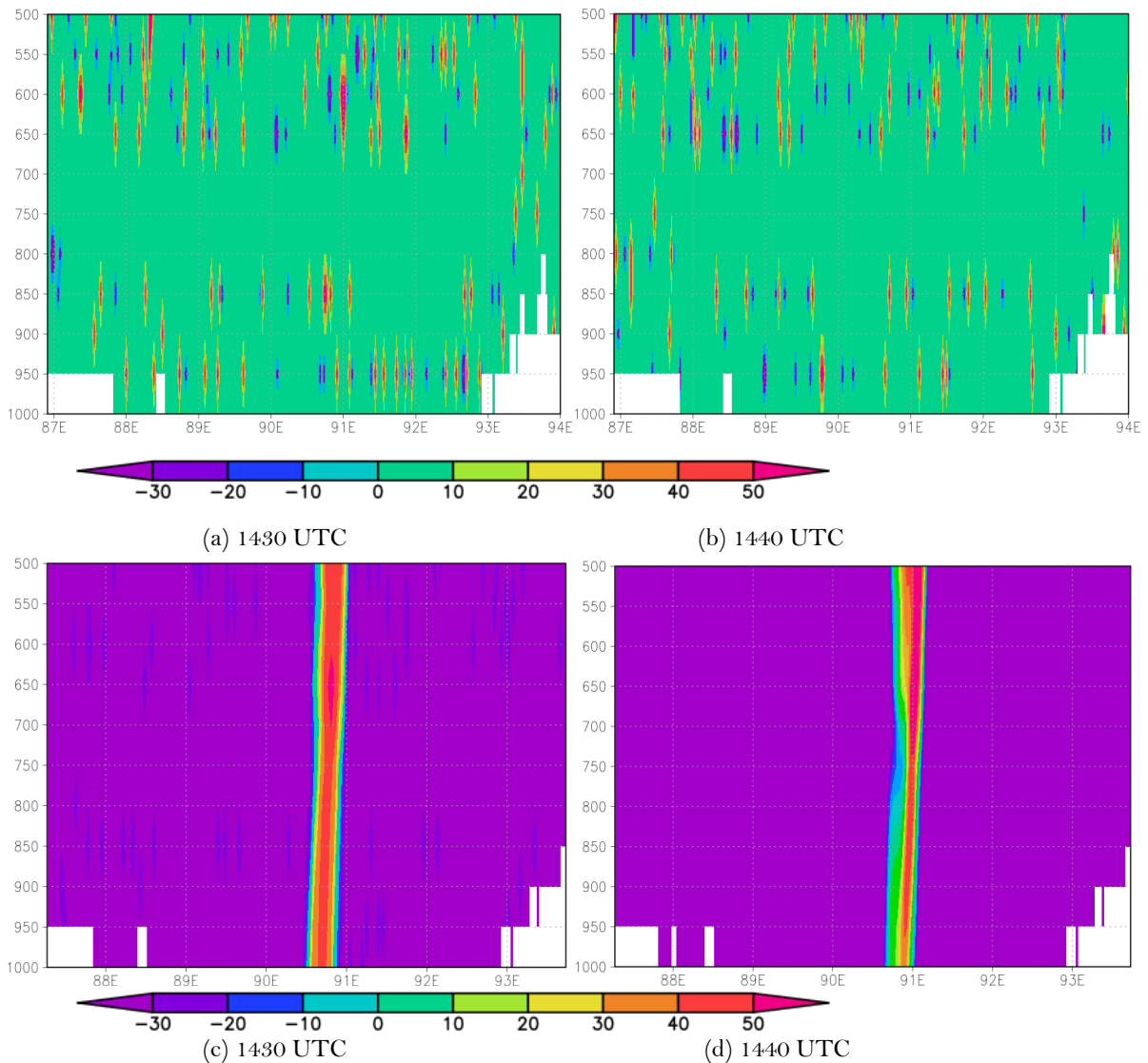


Figure-8. Simulated vertical cross-section of dBZ along 24.89°N for domain  $D_{22}$  (a, b) and domain  $D_{33}$  (c, d).

From Figure 8 (a, b), it is evident that no significant reflectivity was noticed over Sylhet in  $D_{22}$ . However, dBZ above 40 was simulated in the neighborhood of Sylhet in  $D_{33}$ , as shown in Figure 7 (c, d). This difference in simulation is more apparent in the simulated vertical cross-sections shown in Figure 8. Along the latitude 24.89°N of Sylhet, the vertical cross-sections from 1000 hPa to 500 hPa level show no conclusive dBZ value in the case of  $D_{22}$  (Figure 8(a, b)). But in the case of  $D_{33}$ , extreme dBZ values are simulated along the vertical line around 91°E which is quite close to Sylhet. Therefore,  $D_{33}$  showed a far better simulation of reflectivity than that of  $D_{22}$ .

### 5.6. Wind Flow

Mid-level wind pattern is an important indicator of the likelihood of a storm. That's why we analyzed the 500 hPa level wind pattern along with the wind speed. The simulations are shown in Figure 9. It is seen in Figure 9 (a, b) that strong westerly wind of speed above  $24 \text{ ms}^{-1}$  ( $86.3 \text{ km h}^{-1}$ ) is simulated over Sylhet in  $D_{22}$  which is a strong indication of very high wind shear that can result into TS formation. However, this feature is not that



obvious in  $D_{33}$  which shows a lower wind speed of around  $19 \text{ ms}^{-1}$  ( $68.4 \text{ km h}^{-1}$ ) over Sylhet. Thus,  $D_{22}$  performed better in this case.

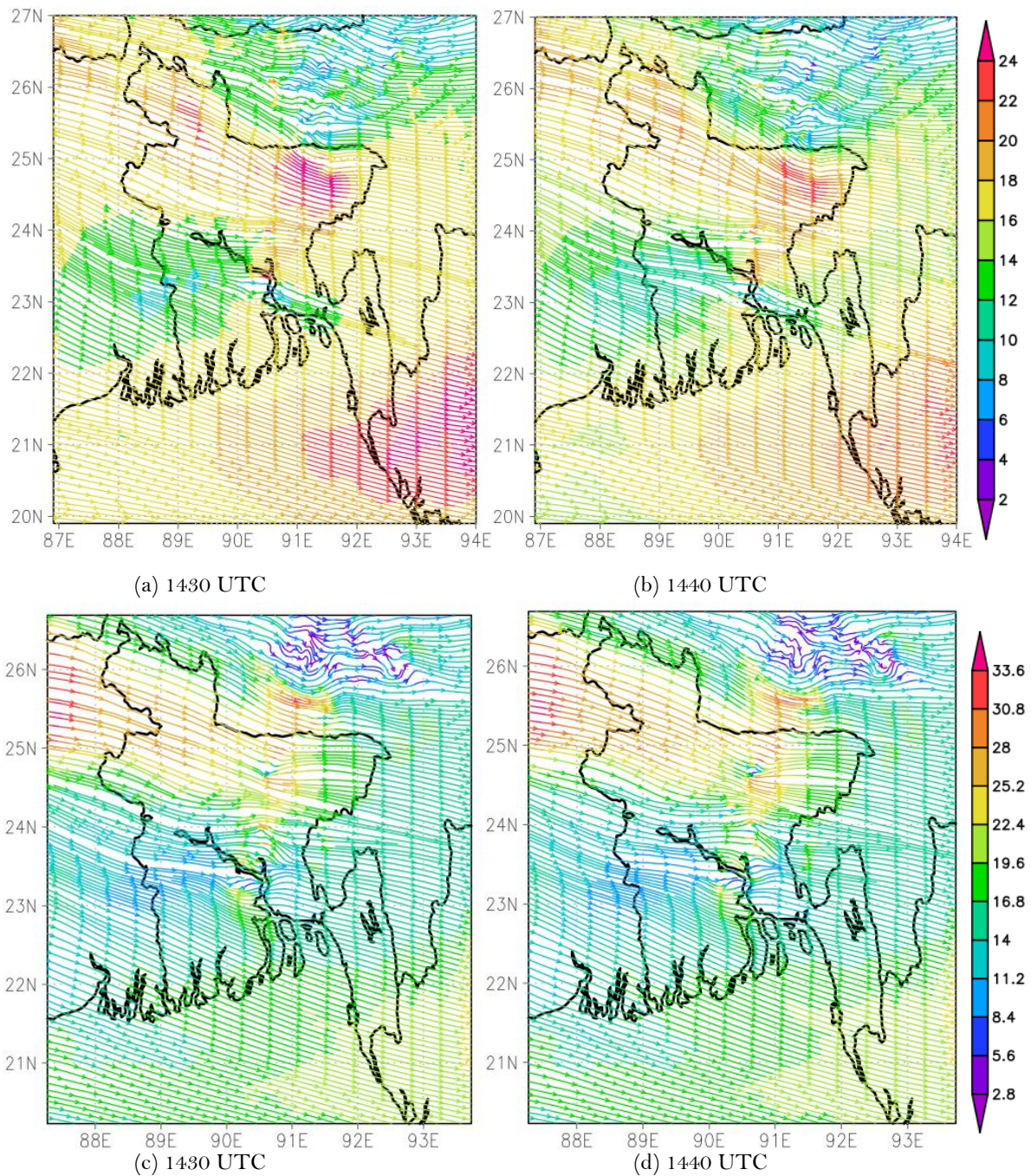


Figure-9. Simulated wind flow and wind speed at 500 hPa level for domain  $D_{22}$  (a, b) and domain  $D_{33}$  (c, d).

## 6. COMPARISONS

### 6.1. Thunderstorm Indicators

An overview of the average of WRF-simulated values of the discussed TS indicators over Sylhet and its neighborhood (from  $24.5^{\circ}\text{N}$  to  $25.5^{\circ}\text{N}$  and  $91.5^{\circ}\text{E}$  to  $92.5^{\circ}\text{E}$ ) at 1440 UTC of 29 March 2018 for both domain  $D_{22}$  and  $D_{33}$  is given in Table 3.

Table-3. Overview of the average WRF-simulated values.

Indicators	$D_{22}$	$D_{33}$	Comment
$CAPE (J kg^{-1})$	879.5	788.3	TS more likely in $D_{22}$
$1 km Hs-r (m^2 s^{-2})$	57.9	85.6	TS more likely in $D_{33}$
$3 km Hs-r (m^2 s^{-2})$	30.5	93.1	TS more likely in $D_{33}$
$KI (°C)$	16.2	28.7	TS more likely in $D_{33}$
$TT (°C)$	50.8	49.9	TS similarly likely in both domains
$Reflectivity (dBZ)$	-28.4	1.4	TS more likely in $D_{33}$
$Wind speed (ms^{-1})$	23.6	18.9	TS more likely in $D_{22}$

## 6.2. Observations

In order to further validate the model performance, simulated values of MSLP, RH, maximum and minimum temperature, and 24-hour rainfall of the event day is compared with the available observations from BMD. The comparison is shown in Figure 10.

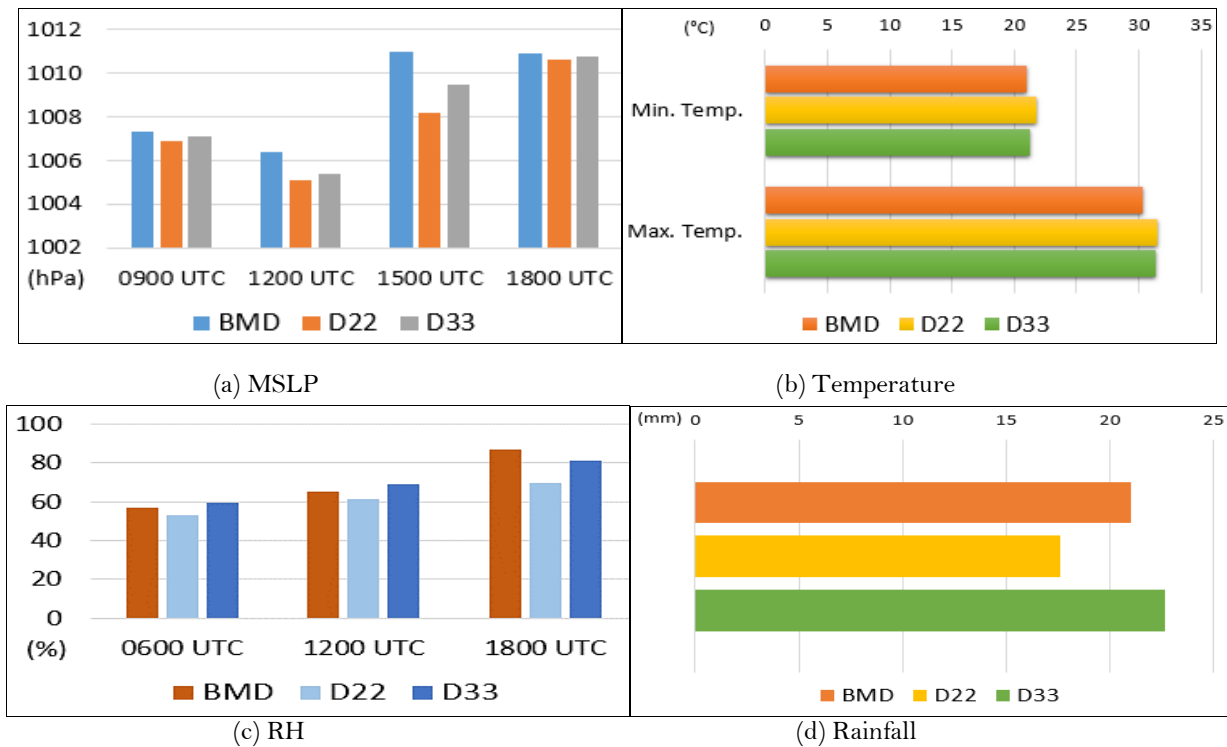


Figure-10. Comparison of model simulations in  $D_{22}$  and  $D_{33}$  with BMD observations: (a) Mean sea level pressure (in hPa), (b) Maximum and minimum temperature (in °C), (c) Relative humidity (in %), and (d) 24-hour rainfall (in mm).

Figure 10 (a) shows that although both  $D_{22}$  and  $D_{33}$  underestimated the actual observations of MSLP,  $D_{33}$  estimates were much closer to the observed values. In Figure 10 (b), however, it is seen that both  $D_{22}$  and  $D_{33}$  overestimated the temperature values in maximum and minimum cases but  $D_{33}$  showed very close approximations. In the case of RH,  $D_{22}$  estimates were much less than the actual records at each time step while the estimations in  $D_{33}$  fluctuated in the close neighborhood of the observations as shown in Figure 10 (c). Finally, in Figure 10(d), it

is found that  $D_{33}$  estimated an amount of around 23 mm rainfall which is much closer to the actual record (21 mm) than that of  $D_{22}$  (around 17 mm). Therefore, it can be said that in each of the comparisons, WRF simulations in  $D_{33}$  were much closer to the actual observations than that of  $D_{22}$ .

## 7. CONCLUSION

From Table 3 and the comparisons with observations in figure 10 (a-d), it can be concluded that the WRF-ARW model simulations of the TS event over Sylhet were better in  $D_{33}$  for almost all of the indicators except for CAPE. That is, the model performed relatively well when the simulations were made over three nested domains instead of two though the horizontal resolution of the innermost domain was 3 km in both cases. Also, the total covered area of the outermost domain was nearly the same. However, it should be noted that before arriving at any conclusive decisions, more case studies over this region need to be analyzed using the WRF model.

**Funding:** This study received no specific financial support.

**Competing Interests:** The authors declare that they have no competing interests.

**Acknowledgement:** All authors contributed equally to the conception and design of the study.

## REFERENCES

- [1] Encyclopedia Britannica Inc, "Thunderstorm." [online]. Retrieved from: <https://www.britannica.com/science/thunderstorm>, 2017.
- [2] M. A. Habib, *Early warning system for severe thunderstorms in Bangladesh*. Dhaka, Bangladesh: In International Forum on Tornado Disaster Risk Reduction for Bangladesh, 2009.
- [3] S. Vaidya, "Simulation of weather systems over Indian region using mesoscale models," *Meteorology and Atmospheric Physics*, vol. 95, pp. 15-26, 2007. Available at: <https://doi.org/10.1007/s00703-006-0188-5>.
- [4] P. Chatterjee, D. Pradhan, and U. K. De, "Simulation of hailstorm event using mesoscale model MM5 with modified cloud microphysics scheme," *Annales Geophysicae*, vol. 26, pp. 3545– 3555, 2008.
- [5] A. J. Litta and U. C. Mohanty, "Simulation of a severe thunderstorm event during the field experiment of STORM programme 2006 using WRF–NMM model," *Current Science*, vol. 95, pp. 204 – 215, 2008.
- [6] B. R. S. B. Basnayake, "SAARC Meteorological Research Centre., Nor'westers over Bangladesh and neighborhood during pre-monsoon season of 2009: Observations and WRF model simulations," SMRC report, 2010, Dhaka: SAARC Meteorological Research Centre2009.
- [7] M. Rajeevan, A. Kesarkar, S. B. Thampi, T. N. Rao, B. Radhakrishna, and M. Rajasekhar, "Sensitivity of WRF cloud microphysics to simulations of severe thunderstorm event over Southeast India," *Annales Geophysicae*, vol. 28, pp. 603– 619, 2010.
- [8] S. Das, "SAARC Meteorological Research Centre., Assimilation of storm 2009 field observations in WRF model and their impact on the simulations of thunderstorms," SMRC Report, 2012, Dhaka: SAARC Meteorological Research Centre2009.
- [9] M. Das, M. Chowdhury, and S. Das, "Sensitivity study with physical parameterization schemes for simulation of mesoscale convective systems associated with squall events," *International Journal of Earth Atmos Sciences*, vol. 2, pp. 20– 36, 2015.
- [10] A. Litta, S. Mary Ididcula, U. Mohanty, and S. Kiran Prasad, "Comparison of thunderstorm simulations from WRF–NMM and WRF–ARW models over east indian region," *The Scientific World Journal*, vol. 2012, pp. 951870–951870, 2012.



- [11] M. Ahasan, D. Quadir, K. Khan, and M. Haque, "Simulation of a thunderstorm event over Bangladesh using wrf-arw model," *Journal of Mechanical Engineering*, vol. 44, pp. 124-131, 2014. Available at: <https://doi.org/10.3329/jme.v44i2.21437>.
- [12] B. K. Bandyopadhyay, M. Mohapatra, L. S. Rathore, and K. Ray, *High-impact weather events over the SAARC Region*: Springer International Publishing, Springer, 2015.
- [13] M. Ahasan and S. Debsarma, "Impact of data assimilation in simulation of thunderstorm (squall line) event over Bangladesh using WRF model, during SAARC-STORM Pilot Field Experiment 2011," *Natural Hazards*, vol. 75, pp. 1009-1022, 2015.
- [14] W. Skamarock, J. B. Klemp, J. Dudhia, D. O. Gill, D. M. Barker, M. G. Duda, X. Y. Huang, W. Wang, and J. G. Powers, "A description of the advanced research WRF version 3 (No. NCAR/TN-475+STR)," University Corporation for Atmospheric Research 2008.
- [15] W. C. Skamarock and M. L. Weisman, "The impact of positive-definite moisture transport on NWP precipitation forecasts," *Monthly Weather Review*, vol. 137, pp. 488-494, 2009. Available at: <https://doi.org/10.1175/2008mwr2583.1>.
- [16] K. V. Ooyama, "A thermodynamic foundation for modeling the moist atmosphere," *Journal of Atmospheric Sciences*, vol. 47, pp. 2580-2593, 1990. Available at: [https://doi.org/10.1175/1520-0469\(1990\)047<2580:atffmt>2.0.co;2](https://doi.org/10.1175/1520-0469(1990)047<2580:atffmt>2.0.co;2).
- [17] R. Laprise, "The Euler equations of motion with hydrostatic pressure as an independent variable," *Monthly Weather Review*, vol. 120, pp. 197-207, 1992. Available at: [https://doi.org/10.1175/1520-0493\(1992\)120<0197:teeomw>2.0.co;2](https://doi.org/10.1175/1520-0493(1992)120<0197:teeomw>2.0.co;2).
- [18] American Meteorological Society, "Glossary of meteorology: Convective available potential energy. Retrieved from: [https://glossary.ametsoc.org/w/index.php?title=Convective\\_available\\_potential\\_energy&oldid=15984#convective\\_available\\_potential\\_energy](https://glossary.ametsoc.org/w/index.php?title=Convective_available_potential_energy&oldid=15984#convective_available_potential_energy)," 2017.
- [19] National Oceanic and Atmospheric Administration, "National weather service glossary: D. Retrieved from: <https://w1.weather.gov/glossary/index.php?letter=d>," 2009.

*Views and opinions expressed in this article are the views and opinions of the author(s), Review of Environment and Earth Sciences shall not be responsible or answerable for any loss, damage or liability etc. caused in relation to/arising out of the use of the content.*